Photon dressed electronic states in topological insulators: Tunneling and conductance

Andrii Iurov[1] *, Godfrey Gumbs[1,2], Oleksiy Roslyak[1], Danhong Huang[3]
[1] *Department of Physics and Astronomy, Hunter College, City University of New York 695 Park Avenue, New York, NY 10065, USA*
[2] *Donostia International Physics Center (DIPC), P de Manuel Lardizabal, 4, 20018 San Sebastian, Basque Country, Spain*
[3] *Air Force Research Laboratory (ARFL/RVSS), Kirtland Air Force Base, NM 87117, USA*
(Dated: March 4, 2013)

The surface bound electronic states of three-dimensional topological insulators, as well as the edge states in two-dimensional topological insulators, are investigated in the presence of a circularly polarized light. The strong coupling between electrons and photons is found t o give rise to an energy gap as well as a unique energy dispersion of the dressed states, different from both graphene and conventional two-dimensional electron gas (2DEG). The effects of electron-photon interaction, barrier height and width on the electron tunneling through a $p-n$ junction and on the ballistic conductance in topological insulators are demonstrated by numerical calculations. A critical energy for an incident electron to tunnel perfectly through a barrier is predicted, where electrons behave as either massless Dirac-like or massive Schrödinger-like particles above or below this threshold value. Additionally, these effects are compared with those in zigzag graphene nanoribbons and a 2DEG. Both the similarities and the differences are demonstrated and explained.

I. INTRODUCTION

The unusual energy band structure of topological insulators (TI), as a novel class of quantum spin materials, has received a considerable amount of theoretical attention in the last few years [1]. The energy dispersion is characterized by an insulating gap in the three-dimensional (3D) bulk states as well as by topologically protected conducting states localized either around the two-dimensional (2D) surface for 3DTIs or around the edge for 2DTIs [2]. In this paper, we adopt the conventional classification (2D/3D) for TIs based on their geometry.

Quantum spin Hall (QSH) topological states were discovered in HgTe/CdTe quantum wells (QWs). The existence of these QSH states is determined by the QW thickness greater than a critical value. For films thicker than 6 nm, such QWs are exemplary 2DTIs but become conventional insulators otherwise [3]. Typical examples of 3DTI include half-space $Bi_{1-x}Sb_x$ alloys as well as Bi_2Se_3, Bi_2Te_3 and Sb_2Te_3 binary crystals. The surfaces of these 3DTIs support spin-polarized Dirac cones analogous to graphene [4,5].

It has been shown that topological states may acquire an energy gap [6,7]. Since it is usually produced as a geometrical gap, it requires a finite size along a given direction. The energy gap depends on either the ribbon width for a QW in 2DTIs or the separation between two surfaces of 3DTIs. For example, a ribbon width of 200 nm produces a gap which is about 0.5 meV. In this paper, we propose another approach for generating an energy gap by coupling the topological surface states to circularly polarized light. This type of dynamic gap was predicted in graphene based on both a semiclassical approach [8] and a quantum mechanical formalism [9–11].

The creation of an energy gap may lead to a metal-insulator phase transition. The conical dispersion of metallic graphene has provided unimpeded electron tunneling through a p-n junctions (Klein paradox) [4,5]. On the other hand, Klein-like total reflection has been predicted for bilayer metallic graphene with its massive but still chiral electrons [12]. Chirality is shown to be the key property for total reflection. However, perfect tunneling may still be expected for certain values of the longitudinal momentum of electrons in the barrier region because these transmission resonances are not affected by the chirality.

The light-induced energy gap is able to break the chirality [13] and suppresses the Klein effect in graphene. In this paper, we would expect that a similar effect may occur in TIs because the helicity of the topological states is also broken by an energy gap. Our numerical results demonstrate a cross-over behavior from Klein-like tunneling in a TI to tunneling of conventional a two-dimensional electron gas (2DEG). Here, by Klein-like we mean that the energy dispersion of topological states deviates from the Dirac cone. For instance, in a 3DTI, there exists an inherent mass term in the effective surface Hamiltonian, which affects the Klein effect in TIs. The interplay between the induced

* E-mail contact: aiurov@hunter.cuny.edu

and inherent mass terms, as well as their competing effects on the electron transmission, are the main subjects of our investigation. In Ref. [14], tunneling and transport problems in the presence of tilted uniform magnetic and electric fields were studied, and we will briefly discuss the effect of the dynamic gap for these cases.

The rest of our presentation is organized as follows. In Sec. II, we first discuss the dressed topological states and obtain their energy dispersion and wave functions for surface states and present an effective surface Hamiltonian as well. Similar to graphene, the quantum field formalism predicts a dynamic gap due to electron-photon coupling. The distorted valence-band dispersion of the TI is calculated and compared to that for graphene with the main focus on broken chiral/helical symmetry. In Secs. III and IV, we explore the effect of an induced gap on electron transmission through a barrier in a TI for incident energies either less or greater than the barrier height. Specifically, Sec. III is devoted to tunneling in 3DTIs along with comparisons to graphene and 2DEG, whereas Sec. IV deals with electron transmission in 2DTIs to complement the results on electron tunneling in zigzag graphene nanoribbons (ZNRs).

II. ELECTRON-PHOTON INTERACTION AND DRESSED STATES

In this section, by including electron-photon coupling, we derive an effective Hamiltonian for surface states of TIs based on quantum field theory. Both the single-mode and double-mode optical fields are considered and their energy dispersions for dressed electron states are compared. Analogous with graphene-like massless particles, the effect of massive particles in TIs on electron states and tunneling are studies.

Let us now consider electron-photon interaction on the surface of a 3DTI. We obtain the dressed electronic states analytically and investigate the tunneling properties of these states. We first assume that the surface of the 3DTI is irradiated by circularly polarized light with its quantized vector potential given by

$$\hat{\mathbf{A}} = \mathcal{F}_0 \left(\mathbf{e}_+ \, \hat{a} + \mathbf{e}_- \, \hat{a}^\dagger \right) \ , \tag{1}$$

where the left and right circular polarization unit vectors are denoted by $\mathbf{e}_\pm = (\mathbf{e}_x \pm i\,\mathbf{e}_y)/\sqrt{2}$, and $\mathbf{e}_x$ ($\mathbf{e}_y$) is the unit vector in the x (y) direction. The amplitude of the circularly polarized light is related to the photon angular frequency ω_0 by $\mathcal{F}_0 \sim \sqrt{1/\omega_0}$. Here, we consider a weak field (energy $\sim \mathcal{F}_0^2$) compared to the photon energy $\hbar\omega_0$. Additionally, the total number N_0 of photons is fixed for the optical mode represented by Eq. (1), corresponding to the case with focused light incident on a portion of an optical lattice modeled by Floquet theory [8].

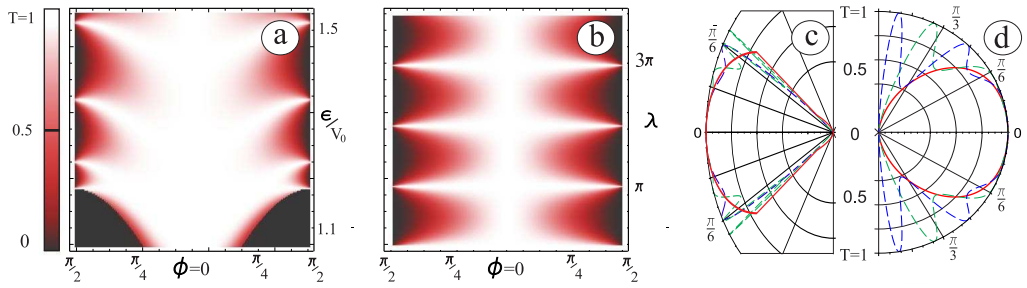

FIG. 1: (Color online) Transmission amplitude $\mathcal{T}$ for Dirac-like surface states for a TI with no quadratic term in the energy dispersion, $\mathcal{D} = 0$. Panels (a) and (b) are density plots of $\mathcal{T}(\phi, \varepsilon)$ for a potential $V(x) = V_0$ and width $W = 50\,\text{nm}$ as well as of $\mathcal{T}(\phi, \lambda)$ for $V(x) = \lambda\,\delta(x)$ when $\varepsilon/V_0 = 1.5$, respectively. Panels (c) and (d) show the ϕ dependence of $\mathcal{T}(\phi, \varepsilon)$ with $W = 50\,\text{nm}$ at $\varepsilon/V_0 = 1.5$ and $\varepsilon/V_0 = 5$, respectively, where the red solid curves are for $W = 50\,\text{nm}$, the blue dashed curves for $W = 150\,\text{nm}$, and the green dashed curves for $W = 250\,\text{nm}$.

The non-interacting Hamiltonian of 3DTI was derived in Ref. [15] and we write it as

$$\mathcal{H}_{3D}^{\text{esm}} = \mathcal{D}k^2 \overleftrightarrow{\mathbb{I}}_{[2]} + \mathcal{A}\overleftrightarrow{\sigma} \cdot \mathbf{k} = \begin{pmatrix} \mathcal{D}k^2 & \mathcal{A}k_- \\ \mathcal{A}k_+ & \mathcal{D}k^2 \end{pmatrix} \ , \tag{2}$$

where $\overleftrightarrow{\mathbb{I}}_{[2]}$ is a 2×2 unit matrix, $\overleftrightarrow{\sigma}$ stands for the usual Pauli matrices, $\mathbf{k}=(k_x,\,k_y)$ is the in-plane surface wave vector with respect to the Γ-point and $k_\pm = k_x \pm i\,k_y$. For the 3DTI considered here, the group velocity is of the same order of magnitude as graphene, i.e., $\mathcal{A}\sim\hbar v_F\sim 10^{-29}\,\mathrm{J{\cdot}m}$. It was shown that the leading quadratic term in Eq. (2) is necessary although the higher order terms with respect to $\mathcal{O}(k^2)$ may be neglected. The massless form of the Hamiltonian in Eq. (2) with no quadratic term, $\mathcal{D}=0$, formally coincides with graphene Dirac cones and retains all graphene electronic properties. Specifically, for electron tunneling, these properties include the absence of back-scattering for head-on collisions (Klein paradox) as well as distinct tunneling resonances in the electron energy distribution.

The energy dispersion relation associated with Eq. (2) is $\varepsilon_{3D}^{\mathrm{surf}}=\mathcal{D}k^2+\beta\mathcal{A}\,|k|$, where $\beta=\pm 1$ is analogous with *pseudo-spin* in graphene. Both $\mathcal{A}$ and $\mathcal{D}$ are independent of wave vector k. This dispersion relation shows that the particle-hole symmetry is broken by virtue of the massive $\mathcal{D}$-term. For completeness, the transmission amplitude of the massless topological states (with $\mathcal{D}=0$) is presented in Fig. 1. Comparing Figs. 1(a) and (b), we clearly see a significant difference although the thickness of a potential barrier is only 50 nm. The effect of coupled dressed states on the tunneling is much stronger for a δ-function barrier. At the same time, the tunneling resonant peaks are broadened significantly compared with graphene. From Figs. 1(c) and (d), we also find that the angular distribution of transmission side-peaks at larger angles displays a non-monotonic dependence on the barrier width W for the higher scaled electron energy $\varepsilon/V_0=5$. In addition, the broadening of resonant peaks at small angles is also significant in comparison with graphene.

The interaction with the optical mode may be introduced into the Hamiltonian in Eq. (2) via a standard transformation of $\mathbf{k}\to\mathbf{k}+e\hat{\mathbf{A}}/\hbar$. In Appendix A, we have shown that this transformation leads to the following effective Hamiltonian, after the field correction has been neglected,

$$\hat{\mathcal{H}}=\hbar\omega_0\,\hat{a}^\dagger\hat{a}+\mathcal{D}k^2\,\overleftrightarrow{\mathbb{I}}_{[2]}+2\zeta\mathcal{D}\left(k_+\hat{a}+k_-\hat{a}^\dagger\right)\overleftrightarrow{\mathbb{I}}_{[2]}+\mathcal{A}\,\overleftrightarrow{\sigma}\cdot\mathbf{k}+2\zeta\mathcal{A}\left(\overleftrightarrow{\sigma}_+\hat{a}+\overleftrightarrow{\sigma}_-\hat{a}^\dagger\right)\,, \tag{3}$$

where we have introduced a small parameter $\zeta=e\mathcal{F}_0/(\sqrt{2}\hbar)$ to describe the light-matter interaction. We assume that the optical mode accommodates a large number N_0 of photons with $N_0\gg 1$. Consequently, all the terms ofder $\zeta^2\sim\mathcal{O}(1/N_0)$ may be neglected. Under these conditions, the energy dispersion associated with Eq. (3) becomes

$$\varepsilon_{3D}^{\mathrm{surf}}(\Delta)=N_0\,\hbar\omega_0+\mathcal{D}k^2+\beta\sqrt{\Delta^2+(\mathcal{A}k)^2} \tag{4}$$

with $\beta=\pm 1$ and the induced energy gap defined by

$$\Delta=\sqrt{\mathcal{W}_0^2+(\hbar\omega_0)^2}-\hbar\omega_0\sim\hbar\omega_0\left(\frac{\alpha^2}{2}\right)\,, \tag{5}$$

where $\alpha=\mathcal{W}_0/(\hbar\omega_0)$ and $\mathcal{W}_0$ is the electron-photon interaction energy. For the upper subband with $\beta=1$ in Eq. (4), the energy gap is related to the effective mass around $\mathbf{k}=0$ through $2m_\Delta^*=\hbar^2/\left[\mathcal{A}^2/(2\Delta)+\mathcal{D}\right]$, where the photon dressing decreases the effective mass. This is in contrast with single-layer graphene, where electron-photon interaction leads to an an effective mass. A similar phenomenon on the effective mass reduction is also found in bilayer graphene under the influence of circularly polarized light. The dressed state wave function corresponding to Eq. (4) is given by

$$\Phi_{\mathrm{e-ph}}^{\mathbf{k}}(x,\,y)=\frac{1}{\sqrt{1+\gamma^2(\beta)}}\begin{pmatrix}1\\ \gamma(\beta)\mathsf{e}^{i\phi}\end{pmatrix}\mathsf{e}^{ik_xx+ik_yy}\,, \tag{6}$$

where $\gamma(\beta)=\mathcal{A}k/[\Delta+\beta\sqrt{\Delta^2+(\mathcal{A}k)^2}]$ and $\phi=\tan^{-1}(k_y/k_x)$. The energy dispersions associated with the Hamiltonian in Eq. (3) [also see Eq. (A17)] for two-mode light interaction with electrons are given by

$$\varepsilon_{\{N_0\uparrow,N_0\downarrow,\,N_0+1\uparrow,N_0+1\downarrow\}}(k,\,\Delta)=\left(N_0+\frac{1}{2}\right)\hbar\omega_0+\mathcal{D}k^2\pm\sqrt{\mathbb{C}_1(k,\,\Delta)\pm\sqrt{\mathbb{C}_2(k,\,\Delta)}}\,, \tag{7}$$

where a doubled state space is used for spanning the Hamiltonian,

$$\mathbb{C}_1(k,\,\Delta)=(\hbar\omega_0/2)^2+\zeta\nu\mathcal{A}\mathcal{D}k^2+[\zeta^2\mathcal{D}^2+\mathcal{A}^2(1+5/2\nu^2)]k^2\,, \tag{8}$$

$$\begin{aligned}\mathbb{C}_2(k,\,\Delta)=&\,\zeta^2\mathcal{A}^2\mathcal{D}^2k^4(1+\nu^2)+4\nu(\zeta\nu\mathcal{D}+\mathcal{A})\mathcal{A}^3k^4\\ &-3\nu(2\zeta\mathcal{D}+\nu\mathcal{A})\mathcal{A}\hbar\omega_0\Delta k^2+4(\hbar\omega_0)^2\left[\Delta^2+(\mathcal{A}k)^2\right]\,,\end{aligned} \tag{9}$$

and $\nu \sim \alpha/2$.

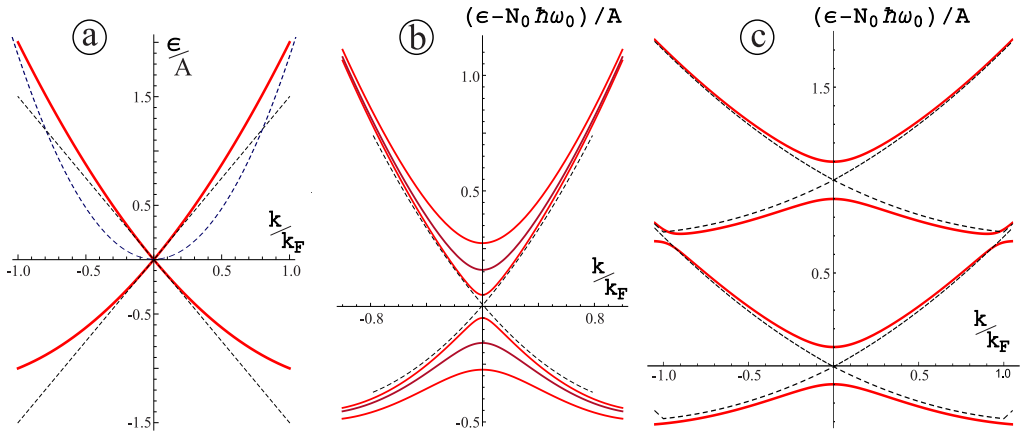

FIG. 2: (Color online) Energy dispersion (red solid curves) for the effective surface model of 3DTI: (a) without light-electron interaction [$\alpha = 0$, $\mathcal{D}k_F^2/(\hbar\omega_0) = \mathcal{A}k_F/(\hbar\omega_0) = 0.2$]; (b) for single-mode dressed states [$\alpha = 0.05$ (inner), 0.07 (middle), 0.1 (outer)] in Eq. (4); and (c) for two-mode dressed states in Eq. (7). Here, the black dashed lines in (a) represent the Dirac cones and a parabola, while the black dashed curves in (b) and (c) indicate the asymptotical behaviors for $\alpha = 0$.

As $\zeta\mathcal{D} \to 0$ and $\nu k \to 0$, the two-mode dressed states become decoupled and are simply given by

$$\varepsilon_{\{N_0\uparrow,\, N_0\downarrow\}}(k,\, \Delta) = N_0\,\hbar\,\omega_0 + \mathcal{D}k^2 \pm \sqrt{\Delta^2 + (\mathcal{A}k)^2}\ , \tag{10}$$

$$\varepsilon_{\{N_0+1\uparrow,\, N_0+1\downarrow\}}(k,\, \Delta) = (N_0+1)\,\hbar\omega_0 + \mathcal{D}k^2 \pm \sqrt{\Delta^2 + (\mathcal{A}k)^2}\ . \tag{11}$$

On the other hand, for single mode dressed states, the effect due to the electron-photon interaction is quite similar to graphene, except that the energy gap varies as α^2. However, this dependence becomes negligible under low -intensity light illumination. The energy dispersion relations for single and double-mode dressed states of 3DTIs are presented in Fig. 2. Comparing Figs. 2(a) and (b), we find that an energy gap is opened at $\mathbf{k} = 0$ due to photon dressing, and the Dirac cone is well maintained except for large k values. In contrast, for double-mode dressed states in Fig. 2(c), additional mini-gaps appear at the Fermi edge and new saddle points are formed at $\mathbf{k} = 0$ due to strong coupling between dressed states with different pseudo-spins. These new mini-gaps and the saddle points prove to have a significant effect on electron tunneling.

The full expression for the 3DTI Hamiltonian which includes the z dependence (perpendicular to the surfaces) may also be related to dressing and can be expressed as [6] (see Eq. (Bin the Appendix)

$$\hat{\mathcal{H}}_{3D}(\mathbf{k}_\perp,\, z) = \hat{\mathcal{H}}^{(1)}_{3D}(z) + \hat{\mathcal{H}}^{(2)}_{3D}(\mathbf{k}_\perp)\ , \tag{12}$$

where

$$\hat{\mathcal{H}}^{(1)}_{3D}(z) = \left(\mathcal{C} - \mathcal{D}_z\partial_z^2\right)\overleftrightarrow{\mathbb{I}}_{[4]} + \begin{pmatrix} (\mathcal{M} + \mathcal{B}_z\partial_z^2)\overleftrightarrow{\sigma}_3 - i\mathcal{A}_z\partial_z\overleftrightarrow{\sigma}_1 & 0 \\ 0 & (\mathcal{M} + \mathcal{B}_z\partial_z^2)\overleftrightarrow{\sigma}_3 + i\mathcal{A}_z\partial_z\overleftrightarrow{\sigma}_1 \end{pmatrix}\ , \tag{13}$$

$$\hat{\mathcal{H}}^{(2)}_{3D}(\mathbf{k}_\perp) = -\mathcal{D}_\perp k^2\overleftrightarrow{\mathbb{I}}_{[4]} - \mathcal{B}_\perp k^2\,\overleftrightarrow{\sigma}_3 \otimes \overleftrightarrow{\mathbb{I}}_{[2]} + \begin{pmatrix} 0 & \mathcal{A}_\perp k_-\overleftrightarrow{\sigma}_1 \\ \mathcal{A}_\perp k_+\overleftrightarrow{\sigma}_1 & 0 \end{pmatrix}\ . \tag{14}$$

In this notation, $\mathbf{k}_\perp = (k_x,\, k_y)$, $\mathcal{C}$, $\mathcal{M}$, $\mathcal{A}_z$, $\mathcal{B}_z$, $\mathcal{D}_z$ are parameters in the Kane $\mathbf{k}\cdot\mathbf{p}$ model for bulk states, and $\mathcal{A}_\perp$, $\mathcal{B}_\perp$, $\mathcal{D}_\perp$ are the parameters for surface states. The corresponding energy dispersion relations are linear and gapless for semi-infinite samples (half-space). However, for a TIs of finite-width, an energy gap is opened due to the finite-size effect. We further find that, similar to graphene, electron-photon interaction may modify the energy gap due to additional contributions from dressing.

III. TUNNELING AND BALLISTIC TRANSPORT IN 3DTI

In this section, we compare surface states of a 3DTI with bilayer graphene in order to find out how w the quadratic term in their energy dispersions influences tunneling. The electron tunneling behaves as massless Dirac fermions

for high incident energies above a critical value, which has been compared with electrons in a graphene layer. On the other hand, the electron tunneling behaves as Schrödinger massive particles at lower incident energies below this critical value, which is similar to the 2DEG. Additionally, the modification from a dressed state energy gap to electron tunneling is investigated for both low and high incident energies.

Let us first turn to the tunneling problem associated with the Hamiltonian in Eq. (2) in the absence of electron-photon coupling. The main input of the p-n junction tunneling is the electron wave function [12,16]

$$\Psi_{\mathbf{k}}(x,\, y) = \frac{1}{\sqrt{2}} \begin{pmatrix} 1 \\ \beta \mathsf{e}^{i\phi} \end{pmatrix} \mathsf{e}^{ik_x x + ik_y y} \ , \tag{15}$$

where $\beta = \pm 1$, as before, and $\phi = \tan^{-1}(k_y/k_x)$. This wave function is simple and chiral, and an eigenstate of the projection of the electron momentum operator along the pseudo-spin direction (chirality/helicity operator) given by $\hat{h} = \overleftrightarrow{\sigma} \cdot \mathbf{p}/(2p)$. For the tunneling process along the x direction, the transverse momentum $\hbar k_y$ is conserved, whereas the longitudinal wave vector component $k_{x,2}$ in the barrier region with $V(x) = V_0$ is determined by

$$k_{x,2}^2 = \left(\frac{-\beta \mathcal{A} + \beta \sqrt{\mathcal{A}^2 + 4\mathcal{D}(\varepsilon - V_0)}}{2\mathcal{D}} \right)^2 - k_y^2 \ . \tag{16}$$

Equation (16) yields not only propagating but also evanescent modes in the barrier region. Moreover, because of the quadratic energy dispersion, both the wave functions and their derivatives need to be matched at boundaries, similar to the tunneling problem with respect to bilayer graphene [12].

Electron tunneling and Andreev reflection for the full 3DTI Hamiltonian was studied in Ref. 17. In the present case, we have $\mathcal{A}/\mathcal{D} \gg k$. Consequently, we may neglect the evanescent contributions. By neglecting the higher-order terms, Eq. (16) is simplified to

$$k_{x,2} = \sqrt{\frac{(\varepsilon - V_0)^2}{2\mathcal{D}(\varepsilon - V_0) + \mathcal{A}^2} - k_y^2} \ . \tag{17}$$

The result for the special case of massless Dirac fermions of graphene may be directly obtained from the above equation after setting $\mathcal{D} \to 0$.

Clearly, from Eq. (17), the electron transmission varies with the incoming particle energy as well as the angle of incidence. There exists a *critical energy* $\varepsilon_{\rm cr} \ll V_0$ above which the transmission behaves like Dirac electrons in graphene. However, particles with incoming energies below this critical value are transmitted like normal Schrödinger electrons in 2DEG. For head-on collisions with $k_y = 0$, the critical energy is calculated to be

$$\varepsilon_{\rm cr} = V_0 - \frac{\mathcal{A}^2}{2\mathcal{D}} \ . \tag{18}$$

The dimensionless two-terminal tunneling conductance, $g(\varepsilon)$, may be calculated from [18]

$$g(\varepsilon) = \frac{\mathcal{G}(\varepsilon)}{2\mathcal{G}_0} = \frac{1}{2} \int\limits_{-\pi/2}^{\pi/2} \mathcal{T}(\phi,\, \varepsilon)\, \cos(\phi)\, d\phi \ . \tag{19}$$

The physical meaning of Eq. (19) is the decrease of the electron conductance in the presence of the barrier due to $\mathcal{T}(\phi,\, \varepsilon) \leq 1$, where $\mathcal{T}(\phi,\, \varepsilon)$ is the transmission probability. According to Ref. [19], $\mathcal{G}_0$ in the case of $\mathcal{D} = 0$ may be estimated using

$$\mathcal{G}_0 = \left(\frac{e^2}{h} \right) \frac{L_y}{2\pi} \int\limits_{-k_F}^{k_F} \frac{dk_y}{\cosh^2(k_y L_x/2)} \ , \tag{20}$$

where k_F is the Fermi wave number and L_x and L_y are the normalization length and width of the sample. When $k_F L_x \ll 1$, we have $\tanh(k_F L_x/2) \approx k_F L_x/2$ and obtain in a straightforward way that $\mathcal{G}_0 = (2e^2/h)\,(L_y/2\pi)\,(\varepsilon_F/\mathcal{A})$ for the Dirac cone with $\varepsilon_F = \mathcal{A}k_F$. In the presence of a small energy gap $\Delta \ll \mathcal{A}k_F$, on the other hand, $\mathcal{G}_0$ is modified to

$$\mathcal{G}_0 = \left(\frac{2e^2}{h}\right) \frac{L_y\sqrt{\varepsilon_F^2 - \Delta^2}}{2\pi\mathcal{A}} \ , \tag{21}$$

where ε_F is the Fermi energy at $k = k_F$.

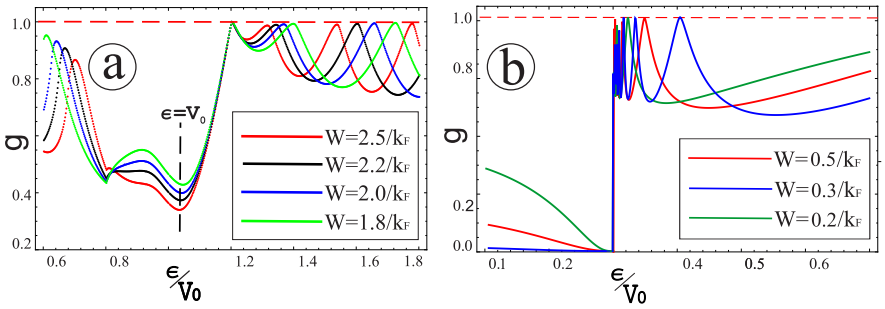

FIG. 3: (Color online) Two-terminal tunneling conductance for the effective surface model of 3DTI with different barrier widths, where $\mathcal{D}k_F/\mathcal{A} = 0.4$. In panels (a) and (b), we present numerical results for tunneling conductance as functions of the incident particle energy for the case of Dirac cone and 3DTI.

The calculated results based on Eq. (19) are presented in Fig, 3. Comparing Figs. 3(a) and (b), we find that the existence of the critical energy in (b) plays a crucial role in the electron tunneling. A series of resonant peaks occur above the critical energy $\varepsilon_{\rm cr}$ in (b) and above the barrier height V_0 in (a) although these two values are quite different. The former is unique to surface states of a massive particle in 3DTI while the latter is related to the transition from Klein tunneling to a regular one for massless fermions in graphene. It is more interesting to notice that the electron tunneling below V_0 in (a) and below the critical energy in (b) is also qualitatively different, where electrons behave like Dirac fermions for Kelin tunneling in (a) and like Schrödinger particle for evanescent wave tunneling in (b). Transition when $\varepsilon = \varepsilon_{\rm cr}$ is extremely sharp in (b).

It is very helpful to compare the results obtained in this section with bilayer graphene having quadratic dispersion. For bilayer graphene, its lowest energy states are described by the Hamiltonian [12]

$$\hat{\mathcal{H}}_{\rm blg} = \frac{\hbar^2}{2m_b}\left(k_-^2\,\overleftrightarrow{\sigma}_+ + k_+^2\,\overleftrightarrow{\sigma}_-\right) \ , \tag{22}$$

where m_b is the effective mass of electrons in the barrier region. In this case, the longitudinal wave vector component in the barrier region is given by

$$k_{x,2}^b = \beta'\sqrt{2m_b\beta(\varepsilon - V_0) - k_y^2} \ , \tag{23}$$

where β', $\beta = \pm 1$. An evanescent wave having a decay rate κ_b can coexist with a propagating wave having wave vector $k_{x,2}$ such that $k_y^2 + k_{x,2}^2 = k_y^2 - \kappa_b^2 = 2m_b\beta(\varepsilon - V_0)$. This implies that the evanescent modes should be taken into account simultaneously. For bilayer graphene, both wave functions and thei derivatives must be continuous at the interfaces. Consequently, the Klein paradox persists in bilayer graphene for chiral but massive particles. However, one finds complete reflection, instead of complete transmission, in this case. This effect has direct links with the specific electron-hole conjugation, i.e. $k_{x,2} \to i\kappa_b$, in the barrier region [12].

To understand the physics for electron tunneling in bilayer graphene, we first present analytical results for single layer graphene, i.e. $\mathcal{D} = 0$. By taking into account all four modes from Eq.(16), for a δ-potential barrier, we obtain the transmission probability as [18]

$$\mathcal{T}_{\delta,\,g} = \frac{1}{1 + \sin^2(\lambda)\,\tan^2(\phi)} \ , \tag{24}$$

reproduces the Klein paradox for the head-on collision corresponding to $\phi = 0$. However, the periodic dependence of the transmission on the scaled barrier strength λ in Eq. (24) is non-trivial. Such perfect tunneling with $\mathcal{T}_{\delta,\,g} = 1$ also exists for a set of λ values when $\sin(\lambda) = 0$ is satisfied. Furthermore, this prediction is consistent with finite-width barrier tunneling [see Fig. 1 (c)]. In fact, the expression in Eq. (24) may be derived directly from the general result for electron transmission through a very high potential barrier with $V_0 \gg \varepsilon$, that is,

$$\mathcal{T}_g = \frac{\cos^2(\phi)}{1 - \cos^2(k_{x,2}W)\,\sin^2(\phi)} = \frac{1}{1 + \sin^2(k_{x,2}W)\,\tan^2(\phi)}\ , \tag{25}$$

where $k_{x,2} \sim -V_0/\mathcal{A}$ is used for $V_0 \gg \varepsilon$. It is clear that λ in Eq. (24) plays the role of $k_{x,2}W$ for a finite barrier width W.

For a conventional 2DEG with a δ-function potential barrier [20], its transmission amplitude is given by $\mathcal{T}_\lambda = 2\hbar^2\varepsilon/(2\hbar^2\varepsilon + m^*\lambda^2 W^2)$. Here, we consider a head-on collision with $k_x = \sqrt{2m^*\varepsilon/\hbar^2}$ and m^* is the electron effective mass. One may easily see that for $\lambda \to 0$ (or a very-thin barrier layer) complete transmission ($\mathcal{T}_\lambda \to 1$) can be obtained. When $\lambda \to \infty$, on the other hand, one gets complete reflection.

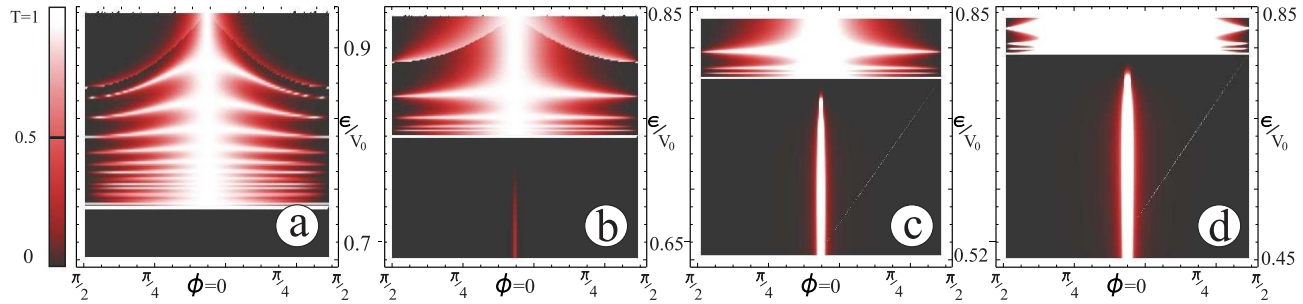

FIG. 4: (Color online) Density plots of the transmission amplitude $\mathcal{T}(\phi,\,\varepsilon)$ for bare electron states with energy gap $\Delta = 0$ in the effective surface model for 3DTI with $(\mathcal{D}/\mathcal{A})\,k = 0.4$. Panels (a), (b), (c) and (d) correspond to $k_{1,\max}W = 2.5$, 1.1, 0.95 and 0.75.

Figure 4 presents our numerical results for the transmission amplitude $\mathcal{T}(\phi,\,\varepsilon)$ for several values of barrier width in the absence of photon dressing or when the coefficient $\Delta = 0$ in the energy dispersion relation. From this figure, we find that the coupling between dressed states with different pseudo-spins is very strong for a double-mode optical field, similar in nature to the result in Fig. 2(c). Here, Dirac-like tunneling above a critical energy may be seen for a thick barrier layer, as described by Eq. (25). Schrödinger-like tunneling below the critical energy, on the other hand, may only be observed for a relatively thin barrier layer under the normal-incidence condition, as discussed for 2DEG with $\lambda \to 0$. With decreased W, electron tunneling below the critical energy is gradually enhanced as $\phi \to 0$. From direct comparison between Fig. 4 and Fig. 1(a) we know that the major effect of the massive $\mathcal{D}$-term on the electron tunneling is associated with the occurrence of a critical energy below which no significant electron tunneling is expected for a thick barrier layer. In addition, the critical energy shifts up with decreasing W and the contribution from the evanescent mode to the transmission is found finite as long as the barrier width W meets the condition $W|\mathrm{Im}(k_{x,2})| < 1$.

We now turn to the model for the 3DTI surface with $\Delta \neq 0$. For this, the longitudinal momentum of electron dressed states may be approximated by

$$k_{x,2}^{\Delta} = \sqrt{\frac{(\varepsilon - V_0)^2 - \Delta^2}{2\mathcal{D}(\varepsilon - V_0) + \mathcal{A}^2} - k_y^2}\ . \tag{26}$$

Numerical results for the transmission amplitudes based on Eq. (26) are presented in Fig. 5, where the same parameters were chosen as those in Fig. 4. Comparing Fig. 5(a) with Fig. 1(a) for $\mathcal{D} = 0$, we find that the effect of a photon-induced energy gap ia to produce additional side peaks in the angle distribution of $\mathcal{T}(\phi,\,\varepsilon)$. After a massive $\mathcal{D}$-term is introduced, as presented in Figs. 5(b)-(d), the side peaks are significantly suppressed and a critical energy appears. At the same time, the Schrödinger-like electron tunneling below this critical energy is also partially suppressed for a thin barrier layer even under the normal-incidence condition by comparing Fig. 5(d) with Fig. 4(d).

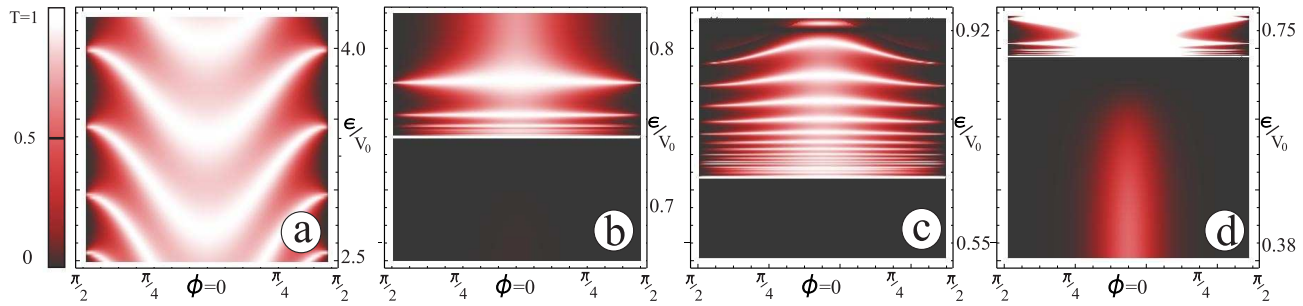

FIG. 5: (Color online) Density plots of the transmission amplitude $\mathcal{T}(\phi,\,\varepsilon)$ for the electron dressed states in the effective surface model of 3DTI with $\Delta/V_0 = 0.2$, $\mathcal{D} = 0$ (Dirac cone) for panel (a) and $(\mathcal{D}/\mathcal{A})\,k = 0.15$ for all other panels. Panels (a), (b), (c) and (d) correspond respectively to $k_{1,\max}W = 1.5$, 1.3, 1.1 and 0.85.

IV. ELECTRON TUNNELING IN 2DTI AND ZNR

In this section, we compare edge states of a 2DTI with a zigzag graphene nanoribbon in order to find any similarities resulting from an induced energy gap in their energy dispersions. At the same time, the dissimilarities between the 2DTI and an armchair graphene nanoribbon is also discussed. Additionally, the effect of the decay of electron wave functions away from the edges on the electron tunneling are investigated both inside and outside the barrier region.

According to the Kane model for a HgTe/CdTe semiconductor quantum well [2,7], the 2DTI system may be effectively described by the following 4×4 matrix Hamiltonian, i.e.,

$$\mathcal{H}_{2D}(k_x,\,y) = \begin{pmatrix} \overleftrightarrow{h}_B(k_x,\,y) & 0 \\ 0 & \overleftrightarrow{h}^{\dagger}_B(k_x,\,y) \end{pmatrix}\,, \tag{27}$$

where

$$\overleftrightarrow{h}_B(k_x,\,y) = \begin{pmatrix} \mathcal{C}+\mathcal{M}-(\mathcal{D}+\mathcal{B})(k_x^2-\partial_y^2) & \mathcal{A}(k_x-i\partial_y) \\ \mathcal{A}(k_x+i\partial_y) & \mathcal{C}-\mathcal{M}-(\mathcal{D}-\mathcal{B})(k_x^2-\partial_y^2) \end{pmatrix}\,, \tag{28}$$

where k_x is assumed small. Additionally, we assumed translational symmetry along the x-axis so that $k_x \to -i\partial_x$. The coefficients $\mathcal{A}$, $\mathcal{B}$, $\mathcal{C}$, $\mathcal{D}$ and $\mathcal{M}$ are expansion parameters within the Kane $\mathbf{k}\cdot\mathbf{p}$ model. Their role in the energy dispersion is such that $\mathcal{M}$ is usually referred to as Dirac mass and $\mathcal{B}$ is called the Newtonian mass. We note that $\mathcal{M}$ changes sign at the critical thinness $d_{\rm cr} \simeq 6.1\,$nm. For a layer with $d > d_c$, $\mathcal{M}$ is negative which is referred to as an *inverted-type* TI.

We note that the Hamiltonian in Eq. (27) is block-diagonal, for which we expect two independent wave functions, Ψ_+ and Ψ_-, corresponding to different directions of the electron spin projection. It is straightforward to show that Ψ_+ and Ψ_- are related to each other by a time-reversal operator [7], i.e. $\Psi_- = -i\overleftrightarrow{\sigma}_y\Psi_+^{\dagger}$. This implies that any transmission associated with Ψ_+ must accompany another transmission of Ψ_- in the opposite direction along the same edge of the 2DTI. For that reason, the eigenstates $\Psi_\pm$ are usually referred to as helical edge states [2]. For all the calculations which follow, we made use of the fact that $\mathcal{C}$ only appears along the diagonal of the matrix in Eq.(28). By making the replacement $\varepsilon \to \varepsilon - \mathcal{C}$, one may show in a straightforward way that the $\mathcal{C}$-term is irrelevant to electron transmission.

Before solving the eigenvalue problem, we estimate [21] all quantities and coefficients in the Hamiltonian in Eqs. (27) and (28) at $d = 5\,$nm ($< d_{\rm cr}$). The range of considered wave vectors is chosen as $k = 10^{-2}\text{Å}^{-1} \ll k_F$. In that range, the parameters appearing in the Hamiltonian are: [2] $\mathcal{C} \simeq 10^{-2}\,$eV, $\mathcal{A}k \simeq \mathcal{B}k^2 \simeq \mathcal{D}k^2 \simeq 10^{-2}eV$. Consequently, each term in the Hamiltonian in Eq. (28) has the same order of magnitude and none of them should be neglected. Since $\mathcal{B} \simeq \mathcal{D}$, we get $\mathcal{B}_+ \equiv \mathcal{B}+\mathcal{D} \simeq 2\mathcal{B}$ and $\mathcal{B}_- \equiv \mathcal{B}-\mathcal{D} \ll \mathcal{B}$.

Apart from those considerations concerning the quantities and coefficients in the Hamiltonian in Eq. (27), the matrix may be separated into two parts. One part depends only on the $y-$coordinate whereas the other one is k_x-dependent. The eigenvalues are determined from the following secular equation

$$\left(\mathcal{M}-\mathcal{B}_{+}(k_x^2-\xi^2)-\varepsilon\right)\left(\mathcal{M}-\mathcal{B}_{-}(k_x^2-\xi^2)-\varepsilon\right)=-\mathcal{A}^2(k_x^2-\xi^2)\ , \tag{29}$$

where ξ characterizes the decay rate of edge state electron wave functions with a finite width in the y direction. After neglecting the $\mathcal{B}_{-}$-term, we obtain from Eq. (29)

$$\xi^2=k_x^2-\frac{(\varepsilon-\mathcal{M})^2}{\mathcal{A}^2-\mathcal{B}_{+}(\varepsilon-\mathcal{M})}\ . \tag{30}$$

The electron wave function, tunneling and transport properties for a system with finite width differ significantly from those of a semi-infinite model because of a gap in the energy dispersion.

In the limiting semi-infinite geometry for a 2DTI, we obtain the following exact 1D effective edge model along the y-direction, [2]

$$\mathcal{H}_{1D}^{\rm eem}=\mathcal{A}k_y\overleftrightarrow{\sigma}_z\ , \tag{31}$$

whose corresponding dispersion relations are $\varepsilon_{1D}^{\rm eem}=\pm\mathcal{A}k_y$ with corresponding wave functions are the eigenfunctions of σ_z, i.e., $\Psi_1^T=\{0,\,1\}$ and $\Psi_2^T=\{1,\,0\}$, which yield a transmission amplitude $\mathcal{T}_{\rm eem}=1$ through a barrier of any height analogous to the Klein paradox for head-on collisions in graphene. In contrast to the 2D model in Eq. (27), we find that the electron transmission for edge states with a finite width is substantially suppressed.

Taking the limit $L_y\to\infty$, we can also consider bulk states which are located far away from either edge. In this case, we make the substitution $k_y=-i\partial_y$. By retaining terms up to order $\mathcal{O}(k^3)$, calculation leads to a new energy dispersion for $\mathcal{A}\gg\mathcal{B}k$

$$\varepsilon_{2D}^{\rm bulk}=-\mathcal{D}k^2\pm\sqrt{\mathcal{M}^2+(\mathcal{A}^2-2\mathcal{M}\mathcal{B})k^2}\ . \tag{32}$$

The Hamiltonian in Eq. (28) assumes the the simple form $\pm\mathcal{M}\overleftrightarrow{\sigma}_z$ at $\mathbf{k}=0$, where the gap parameter $\mathcal{M}$ strongly depends on the thickness d of the quantum well and can be arbitrarily small or even set equal to zero. The energy dispersion relations in Eq. (32) formally reduce to those of gapped graphene or graphene irradiated with circularly polarized light. The tunneling problems for this case were addressed in Refs. [18] and [13]. The most significant effect of radiation on electron tunneling is the breaking of chiral symmetry on the order of $\mathcal{O}(\mathcal{M}^2)$. Consequently, significantly different behavior in the electron transmission at small incident angles ($|k_y|\ll|k_x|$) is expected compared to infinite graphene in the absence of light illumination [12].

As derived from Ref.[7], the decay rates $\xi_{1,2}$ introduced in Eq. (29) are given by

$$\xi_{1,2}=\frac{\mathcal{A}\sqrt{1-(\mathcal{D}/\mathcal{B})^2}}{2(\mathcal{B}+\mathcal{D})}\pm\frac{\sqrt{\mathcal{A}^2(\mathcal{B}-\mathcal{D})-4\mathcal{B}\mathcal{M}(\mathcal{B}+\mathcal{D})}}{2\mathcal{B}\sqrt{\mathcal{B}+\mathcal{D}}}\ . \tag{33}$$

The above equation, in conjunction with Eq. (29), leads to the following energy dispersion relations

$$\varepsilon_\beta+\frac{\mathcal{M}\mathcal{D}}{\mathcal{B}}=\beta\sqrt{\Delta_z^2+\left[\frac{\mathcal{A}}{\mathcal{B}^2}(\mathcal{B}^2-\mathcal{D}^2)\,k_x\right]^2}+\mathcal{O}(k_x^2)\ , \tag{34}$$

where Δ_z is defined by[7]

$$\Delta_z=\frac{4\mathcal{A}\mathcal{M}(\mathcal{B}^2-\mathcal{D}^2)}{\mathcal{B}^3[\mathcal{A}^2\mathcal{B}-4\mathcal{M}(\mathcal{B}^2-\mathcal{D}^2)]}\ . \tag{35}$$

Additionally, the transposed wave function associated with $\xi_{1,2}$ under the limit of $\xi_{1,2}L_y\gg1$ is

$$\Psi_\beta^T(y)=\frac{\mathsf{e}^{ik_xx}}{\mathcal{N}}\{f_{\rm e}-\beta s_k f_{\rm o},\,\frac{(\mathcal{B}+\mathcal{D})\,(\xi_1+\xi_2)}{\mathcal{A}}(f_{\rm o}+\beta s_k f_{\rm e})\}\ , \tag{36}$$

with the notation $\beta = \pm 1$, $s_k = \pm 1$, $\mathcal{N}$ is the normalization factor, and we express the wave function components in terms of odd ($f_{\rm o}$ with $-$) and even ($f_{\rm e}$ with $+$) functions, defined by [7]

$$f_{\rm e(o)}(y) = \frac{{\rm e}^{\xi_1 y} \pm {\rm e}^{-\xi_1 y}}{{\rm e}^{\xi_1 L_y/2} \pm {\rm e}^{-\xi_1 L_y/2}} - \frac{{\rm e}^{\xi_2 y} \pm {\rm e}^{-\xi_2 y}}{{\rm e}^{\xi_2 L_y/2} \pm {\rm e}^{-\xi_2 L_y/2}} \ . \tag{37}$$

We now turn to a comparison of the electron tunneling in 2DTI with graphene zigzag nanoribbon (ZNR) quasi-1D edge states. In Ref. [22], the authors calculated the ZNR wave functions as

$$\Psi^{\beta}_{\rm ZNR}(k_x,\, y) = \begin{pmatrix} \beta {\rm e}^{i\pi/2} \sinh[\lambda_{y,n}(L_y/2 + y)] \\ \sinh[\lambda_{y,n}(L_y/2 - y)] \end{pmatrix} \ , \tag{38}$$

where $\lambda_{y,n}$ is related to the edge distribution of electron wave functions. The boundary conditions are such that each of the wave function components vanishes at one of the two ribbon edges (zigzag configuration). This leads to the following relation

$$\frac{k_x - \lambda_{y,n}}{k_x + \lambda_{y,n}} = {\rm e}^{-2\lambda_{y,n} L_y} \ . \tag{39}$$

Equation (39) demonstrates that the real solutions for $\lambda_{y,n}$ exist only if both the conditions $k_x > \lambda_{y,n}$ and $L_y \lambda_{y,n} > 1$ are satisfied. We will assume the ribbon is sufficiently wide so that $k_x L_y > 1$ for k_x in the range of interest. For real $\lambda_{y,n}$, the edge states decay exponentially with decay length $1/\lambda_{y,n}$. This situation is similar to the case of 2DTI discussed above in this section. However, the traverse wave function distribution is drastically different from a graphene armchair nanoribbon (ANR) which has a plane-wave type wave function $\Psi_{\rm ANR}(y) \sim {\rm e}^{ik_y y}$. We also note from Eq. (39) that for large k_x one gets $\lambda_{y,n} \approx 0$, i.e., fast moving electrons with large longitudinal momenta have a negligible decay rate. Therefore, the wave function in this case extends far away from the ribbon edges. For chosen ribbon width, there exists a maximum value for the decay rate.

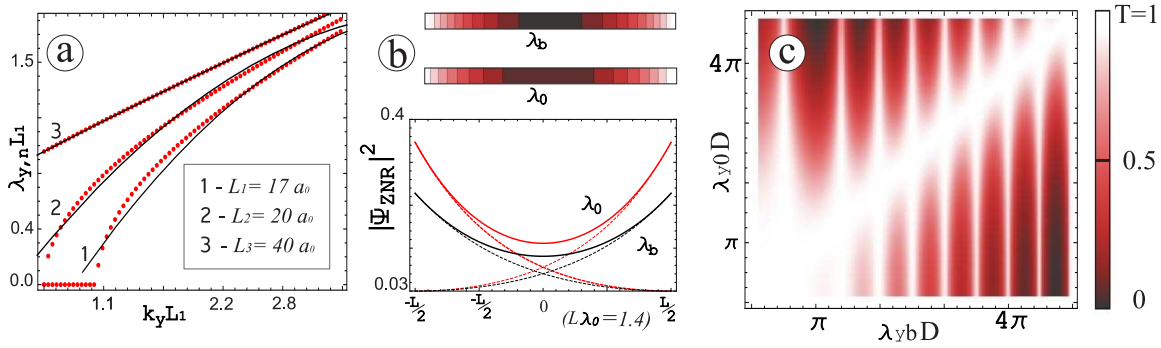

FIG. 6: (Color online) Zigzag nanoribbon wave function and tunneling conductance. Panel (a) demonstrates transverse decay rates $\lambda_{y,n}$ depending on the longitudinal momentum k_x for various nanoribbon widths. Panel (b) shows the y-dependence of the edge state wave functions inside the barrier region (λ_b) and outside the barrier region (λ_0), as well as contour plots of wave functions. Panel (c) presents density plot for the dependence of two-terminal conductance $g(\varepsilon)$ on λ_0 and λ_b.

The energy dispersion for ZNR corresponding to Eq. eqrefznrl is given by $\varepsilon^{\rm ZNR}_{\beta} = \beta\sqrt{k_x^2 - \lambda_{y,n}^2}$. We confine our attention to low potential barriers, such that $\lambda_{y,n}$ is real within a barrier region. Unimpeded tunneling in ZNR was investigated in Ref. [23]. Additionally, we calculated the two-terminal tunneling conductance by making use of

$$g(\varepsilon) = \frac{\mathcal{G}(\varepsilon)}{\mathcal{G}_0} = \frac{1}{L_y} \int\limits_{-L_y/2}^{L_y/2} \mathcal{T}(\varepsilon,\, y)\, dy \ , \tag{40}$$

showing how the ribbon conductivity is modified by a barrier region.

From Fig. 6(a), we find that the wave-function transverse decay length $\lambda_{y,n}^{-1}$ decreases with increasing width of a zigzag nanoribbon. Figure 6(b) show us that the minima of edge-state wave functions in the transverse direction are at the center ($y = 0$) for both inside and outside barrier regions. Furthermore, the wave functions are symmetric with respect to $y = 0$. Our numerical results based on Eq. (40) are presented in Fig. 6(c). The diagonal line in Fig. 6(c) reflects the fact that $\mathcal{T}(\varepsilon, y) \equiv 1$ [or $g(\varepsilon) \equiv 1$] for the same decay rates $\lambda_0 = \lambda_b$. The periodic resonant peaks with respect to λ_b can be clearly seen in Fig. 6(c) similar to the prediction by Eq. (24).

V. CONCLUDING REMARKS

In summary, we have analytically obtained the energy dispersion relations as well as the wave functions of electron dressed states in TIs irradiated by circularly polarized light. A number of helical systems, such as graphene, nanoribbons and topological insulators, are compared . Similar to graphene, the electron-photon coupling in TI leads to a energy gap in the electron energy dispersion relations and eigenstates with the broken chirality symmetry. The tunneling over a square potential barrier is modified significantly if there exists a gap in the energy dispersion of electrons. The combination of Schrödinger-like (massive) and Dirac-like (massless) electrons tunneling below and above a critical energy gives rise to very novel properties. We have further found that some lower energy subbands become nearly dispersiveless with increasing light intensity, which results in unusual electronic properties non-e in graphen

As shown in Ref. [9] for graphene, laser power 10^2 W may produce an energy gap $\Delta \sim 10 - 100$ meV required for making the effect noticeable for THz light frequencies at room temperature. Since the linear-term coefficient (group velocities) of the 3DTI Hamiltonian has the same order of magnitude as graphene, we expect that an experimental verification to be possible.

Although the linear term in the energy dispersion of 3DTIs gives spin-polarized Dirac cones with chirality of the corresponding eigenstates, the appearance of a quadratic term introduces additional effects on electron tunneling. Our calculations for electron tunneling through a square potential barrier indicate that electrons may be transmitted either like chiral particles as they do in graphene or like conventional 2DEG electrons, depending on the incident particle energy above or below a critical energy.

We have also investigated tunneling properties of edge states for massive particles in 2DTIs, such as HgTe/CdTe quantum wells, where an energy gap is introduced by the finite width of samples [7]. From the analysis of dressed edge-state wave function in the presence of circularly polarized light, we have found that particles can always freely propagate along the ribbon edges, which is similar to zigzag graphene nanoribbons but different from semi-infinite 2DTIs where either perfect transmission or complete reflection is obtained for electron-electron and electron-hole transitions, respectively. Although the wave functions in both 2DTI and zigzag ribbons are localized around the edges, the decay rate of edge state wave functions of 2DTI does not depend on the longitudinal wave number, in contrast to the decay rate in a zigzag ribbon.

ACKNOWLEDGEMENTS

This research was supported by contract # FA 9453-11-01-0263 of AFRL. DH would like to thank the Air Force Office of Scientific Research (AFOSR) for its support. The authors also acknowledge considerable contribution and helpful discussions with Liubov Zhemchuzhna.

Appendix A: Model of 3DTI Surface Irradiated with Circularly Polarized Light

Tthe Hamiltonian describing the surface states (at $z = 0$) of a 3DTI to order of $\mathcal{O}(k^2)$ is given by

$$\mathcal{H}_{3D}^{\rm surf} = \mathcal{D}k^2 + \mathcal{A}\overleftrightarrow{\sigma}\cdot\mathbf{k} = \begin{pmatrix} \mathcal{D}k^2 & \mathcal{A}k_- \\ \mathcal{A}k_+ & \mathcal{D}k^2 \end{pmatrix}, \tag{A1}$$

where $\mathbf{k} = (k_x, k_y)$ is the un-plane surface wave vector and $k_\pm = k_x \pm ik_y$. The energy dispersion associated with this Hamiltonian is given by $\varepsilon_{3D}^{\rm surf} = \mathcal{D}k^2 + \beta\mathcal{A}k$ with $\beta = \pm 1$.

We now turn to the case when the surface of the 3DTI is irradiated by circularly polarized light with vector potential

$$\hat{\mathbf{A}} = \mathcal{F}_0 \left(\mathbf{e}_+ \hat{a} + \mathbf{e}_- \hat{a}^\dagger\right) \ , \tag{A2}$$

where $\mathbf{e}_\pm = (\mathbf{e}_x \pm i\mathbf{e}_y)/\sqrt{2}$, $\mathbf{e}_x$ and $\mathbf{e}_y$ are unit vectors in the x and y direction, respectively. Consequently, the in-plane components of the vector potential may be expressed as

$$\hat{A}_x = \frac{\mathcal{F}_0}{\sqrt{2}}(\hat{a} + \hat{a}^\dagger) \ , \qquad \hat{A}_y = i\frac{\mathcal{F}_0}{\sqrt{2}}(\hat{a} - \hat{a}^\dagger) \ . \tag{A3}$$

In order to include electron-photon coupling, we make the following substitutions for electron wave vector

$$\begin{aligned}
k_x \longrightarrow k_x + \frac{e\hat{A}_x}{\hbar} = k_x + \frac{e\mathcal{F}_0}{\sqrt{2}\hbar}(\hat{a} + \hat{a}^\dagger) \ , \\
k_y \longrightarrow k_y + \frac{e\hat{A}_y}{\hbar} = k_y + i\frac{e\mathcal{F}_0}{\sqrt{2}\hbar}(\hat{a} - \hat{a}^\dagger) \ , \\
k_+ \longrightarrow k_+ + \frac{\sqrt{2}e\mathcal{F}_0}{\hbar}\,\hat{a}^\dagger, \qquad k_- \longrightarrow k_- + \frac{\sqrt{2}e\mathcal{F}_0}{\hbar}\,\hat{a} \ , \\
k^2 = k_+k_- \longrightarrow k^2 + \frac{\sqrt{2}e\mathcal{F}_0}{\hbar}\left(k_+\hat{a} + k_-\hat{a}^\dagger\right) + \left(\frac{\sqrt{2}e\mathcal{F}_0}{\hbar}\right)^2 \hat{a}^\dagger\hat{a} \ .
\end{aligned} \tag{A4}$$

In our investigation, we consider high intensity light with $N_0 = \langle \hat{a}^\dagger\hat{a}\rangle \gg 1$, and then, $\hat{a}\hat{a}^\dagger \sim \hat{a}^\dagger\hat{a}$ due to $\hat{a}\hat{a}^\dagger = \hat{a}^\dagger\hat{a} + 1$ for bosonic operators. We adopt this simplification only for the second-order terms $\sim \left(\sqrt{2}e\mathcal{F}_0/\hbar\right)^2$ but not for the principal ones containing $\hbar\omega_0$. With the aid of these substitutions, the Dirac-like contribution to the Hamiltonian in Eq. (A1) becomes

$$\begin{aligned}
\mathcal{H}_{\text{Dirac}} = \mathcal{A}\overleftrightarrow{\sigma}\cdot\mathbf{k} = \mathcal{A}\left(\overleftrightarrow{\sigma}_- k_+ + \overleftrightarrow{\sigma}_+ k_-\right) \\
\longrightarrow \mathcal{A}\left(\overleftrightarrow{\sigma}_- k_+ + \overleftrightarrow{\sigma}_+ k_-\right) + \frac{\sqrt{2}e\mathcal{F}_0}{\hbar}\,\mathcal{A}\left(\overleftrightarrow{\sigma}_-\hat{a}^\dagger + \overleftrightarrow{\sigma}_+\hat{a}\right) \ ,
\end{aligned} \tag{A5}$$

where $\overleftrightarrow{\sigma}_\pm = (\overleftrightarrow{\sigma}_x \pm i\overleftrightarrow{\sigma}_y)/2$. To describe a full electron-photon coupled system, we also need to take into account the photon energy term $\hbar\omega_0\,\hat{a}^\dagger\hat{a}$. This yields

$$\begin{aligned}
\hat{\mathcal{H}} = \left(\hbar\omega_0 + 4\mathcal{D}\zeta^2\right)\hat{a}^\dagger\hat{a} + \mathcal{D}k^2\overleftrightarrow{\mathbb{I}}_{[2]} + 2\zeta\mathcal{D}\left(k_+\hat{a} + k_-\hat{a}^\dagger\right)\overleftrightarrow{\mathbb{I}}_{[2]} \\
+\mathcal{A}\left(\overleftrightarrow{\sigma}_+ k_- + \overleftrightarrow{\sigma}_- k_+\right) + 2\zeta\mathcal{A}\left(\overleftrightarrow{\sigma}_+\hat{a} + \overleftrightarrow{\sigma}_-\hat{a}^\dagger\right) \ ,
\end{aligned} \tag{A6}$$

where $\zeta = e\mathcal{F}_0/(\sqrt{2}\hbar)$. We may also rewrite the Hamiltonian in Eq. (A6) in matrix form as

$$\begin{aligned}
\hat{\mathcal{H}} = \left(\hbar\omega_0 + 4\mathcal{D}\zeta^2\right)\hat{a}^\dagger\hat{a} + \underline{\mathbf{1}} + \underline{\mathbf{2}} + \underline{\mathbf{3}} \\
\equiv \left(\hbar\omega_0 + 4\mathcal{D}\zeta^2\right)\hat{a}^\dagger\hat{a} + \begin{pmatrix} \mathcal{D}k^2 & \mathcal{A}k_- \\ \mathcal{A}k_+ & \mathcal{D}k^2 \end{pmatrix} \\
+2\zeta\mathcal{D}\begin{pmatrix} (k_-\hat{a}^\dagger + k_+\hat{a}) & 0 \\ 0 & (k_-\hat{a}^\dagger + k_+\hat{a}) \end{pmatrix} + 2\zeta\mathcal{A}\begin{pmatrix} 0 & \hat{a} \\ \hat{a}^\dagger & 0 \end{pmatrix} \ ,
\end{aligned} \tag{A7}$$

where $\underline{\mathbf{1}} \equiv \hat{\mathcal{H}}_{3D}^{\text{surf}}$ denotes the initial surface Hamiltonian with no electron-photon interaction, $\underline{\mathbf{3}}$ gives the principal effect due to light coupled to electrons (the only non-zero term at $\mathbf{k} = 0$) and $\underline{\mathbf{2}}$ is the leading term demonstrating the difference between dressed states in graphene and 3DTI.

We know from Eq. (A7) that the Hamiltonian at $\mathbf{k} = 0$ reduces to the exactly solvable Jayness-Cummings model, after we neglect the field correction on the order of $\mathcal{O}(\zeta^2)$. We obtain

$$\hat{\mathcal{H}}_{\mathbf{k}=0} = \hbar\omega_0\,\hat{a}^\dagger\hat{a} + 2\zeta\mathcal{A}\left(\overleftrightarrow{\sigma}_+\hat{a} + \overleftrightarrow{\sigma}_-\hat{a}^\dagger\right) \ . \tag{A8}$$

Following the method adopted in Refs. [9] and [13], we expand the eigenfunctions of Eq. (A8) as

$$|\Psi^0_{\uparrow,N_0}\rangle = \mu_{\uparrow,N_0}|\uparrow,N_0\rangle + \nu_{\uparrow,N_0}|\downarrow,N_0+1\rangle \ ,$$
$$|\Psi^0_{\downarrow,N_0}\rangle = \mu_{\downarrow,N_0}|\downarrow,N_0\rangle - \nu_{\downarrow,N_0}|\uparrow,N_0-1\rangle \ . \tag{A9}$$

By using the properties

$$\hat{a}^\dagger\,|\uparrow\downarrow,N_0\rangle = \sqrt{N_0+1}\,|\uparrow\downarrow,N_0+1\rangle \ ,$$
$$\hat{a}\,|\uparrow\downarrow,N_0\rangle = \sqrt{N_0}\,|\uparrow\downarrow,N_0-1\rangle \ ,$$
$$\overleftrightarrow{\sigma}_\pm\,|\downarrow\uparrow,N_0\rangle = (1-\delta_{\uparrow,+})(1-\delta_{\downarrow,-})\,|\uparrow\downarrow,N_0\rangle \ , \tag{A10}$$

we obtain the energy eigenvalues

$$\frac{\varepsilon^0_\pm}{\hbar\omega_0} = N_0 \pm \frac{1}{2} \mp \frac{1}{2}\sqrt{1+\frac{\alpha^2}{N_0}\left(N_0+\frac{1}{2}\pm\frac{1}{2}\right)}$$
$$\simeq N_0 \pm \frac{1}{2} \mp \left(\frac{1}{2}+\frac{1}{4}\,\alpha^2\right) = N_0 \mp \frac{\alpha^2}{4} \ , \tag{A11}$$

where $\alpha^2 = 2\zeta\mathcal{A}N_0/(\hbar\omega_0)$ with $N_0 \gg 1$. The energy gap at $\mathbf{k}=0$ has been calculated as $\Delta^0 \equiv \varepsilon^0_- - \varepsilon^0_+ \approx (\alpha^2/2)\,\hbar\omega_0$. We note that there is no difference between graphene and the surface states of 3DTI at $\mathbf{k}=0$, and therefore, the result in Refs. [9] and [24] are relevant to each other.

The expansion coefficients in Eq. (A9) are calculated as

$$\mu_{\uparrow\downarrow,N_0} = \sqrt{\frac{1+\Sigma_{\uparrow\downarrow,N_0}}{2\,\Sigma_{\uparrow\downarrow,N_0}}} \ , \qquad \nu_{\uparrow\downarrow,N_0} = \sqrt{\frac{1-\Sigma_{\uparrow\downarrow,N_0}}{2\,\Sigma_{\uparrow\downarrow,N_0}}} \ , \tag{A12}$$

where

$$\Sigma_{\uparrow\downarrow,N_0} = \sqrt{1-\frac{\alpha^2}{N_0}\left(N_0+\frac{1}{2}\pm\frac{1}{2}\right)} \ . \tag{A13}$$

In all further calculations in this Appendix, we assume $\alpha \ll 1$ and $N_0 \gg 1$, corresponding to a larger number of lase photons but weak light coupling to electrons as a perturbation to the electron energy. This leads to the following approximate expressions

$$\mu_{\uparrow,N_0} \simeq \mu_{\downarrow,N_0} \simeq \mu_{\uparrow,N_0+1} \simeq \mu_{\downarrow,N_0+1} \simeq 1-\frac{\alpha^2}{4} \ , \tag{A14}$$

$$\nu_{\uparrow,N_0} \simeq \nu_{\downarrow,N_0} \simeq \nu_{\uparrow,N_0+1} \simeq \nu_{\downarrow,N_0+1} \simeq \frac{\alpha}{2} \ . \tag{A15}$$

Consequently, we only need to keep one pair of index-free coefficients $\{\mu,\nu\}$ such that $\mu = \cos(\Phi)$, $\nu = \sin(\Phi)$ with $\Phi = \tan^{-1}(\alpha/2)$. Furthermore, from the first equity in Eq. (A11), it follows that the energy gap still depends on N_0 in general. However, the difference $\Delta^0_{N_0+1} - \Delta^0_{N_0} \sim \Delta^0/N_0$ is so small that we neglect it for $N_0 \gg 1$.

Generalizing Eq. (A9), we still expand the wave function $\Psi_{\mathbf{k}}$ over the eigenstates of the Hamiltonian in Eq. (A8) for $\mathbf{k} \neq 0$, i.e.

$$|\Psi_{\mathbf{k}}\rangle = \sum_{j=N_0}^{N_0+1}\sum_{\uparrow,\downarrow}\Xi^{\mathbf{k}}_{\uparrow\downarrow,j}|\Psi^0_{\uparrow\downarrow,j}\rangle$$
$$= \Xi^{\mathbf{k}}_{\uparrow,N_0}|\Psi^0_{\uparrow,N_0}\rangle + \Xi^{\mathbf{k}}_{\downarrow,N_0}|\Psi^0_{\downarrow,N_0}\rangle + \Xi^{\mathbf{k}}_{\uparrow,N_0+1}|\Psi^0_{\uparrow,N_0+1}\rangle + \Xi^{\mathbf{k}}_{\downarrow,N_0+1}|\Psi^0_{\downarrow,N_0+1}\rangle \ . \tag{A16}$$

Using Eq. (A16) we project the full Hamiltonian in Eq. (A6) onto the representation $\{\Xi^{\mathbf{k}}_{\uparrow,N_0}, \Xi^{\mathbf{k}}_{\downarrow,N_0}, \Xi^{\mathbf{k}}_{\uparrow,N_0+1}, \Xi^{\mathbf{k}}_{\downarrow,N_0+1}\}$. This yields

$$\left(\begin{array}{cc|cc} N_0\,\hbar\omega_0+\mathcal{D}k^2-\Delta & \mu^2\mathcal{A}k_- & \mu\nu\mathcal{A}k_+-2\zeta\mathcal{D}k_+ & 0 \\ \mu^2\mathcal{A}k_+ & N_0\,\hbar\omega_0+\mathcal{D}k^2+\Delta & 0 & -2\nu\mu\mathcal{A}k_+-2\zeta\mathcal{D}k_+ \\ \hline \nu\mu\mathcal{A}k_--2\zeta\mathcal{D}k_- & 0 & (N_0+1)\,\hbar\omega_0+\mathcal{D}k^2-\Delta & \mu^2\mathcal{A}k_- \\ 0 & -2\nu\mu\mathcal{A}k_--2\zeta\mathcal{D}k_- & \mu^2\mathcal{A}k_+ & (N_0+1)\,\hbar\omega_0+\mathcal{D}k^2+\Delta \end{array}\right) , \tag{A17}$$

where $\Delta \approx \Delta^0$ is the energy gap at $\mathbf{k} \neq 0$ and we have employed the relations for $N = N_0$ or $N_0 + 1$

$$\overleftrightarrow{\sigma}\cdot\mathbf{k}\,|\Psi^0_{\uparrow N}\rangle = \overleftrightarrow{\sigma}\cdot\mathbf{k}\,\{\mu|\uparrow,N\rangle+\nu|\downarrow,N+1\rangle\} = \mu k_+|\downarrow,N\rangle+\nu k_-|\uparrow,N+1\rangle\ , \tag{A18}$$

$$\overleftrightarrow{\sigma}\cdot\mathbf{k}\,|\Psi^0_{\downarrow N}\rangle = \overleftrightarrow{\sigma}\cdot\mathbf{k}\,(\mu|\downarrow,N\rangle-\nu|\uparrow,N-1\rangle) = \mu k_-|\uparrow,N\rangle-\nu k_+|\downarrow,N-1\rangle\ , \tag{A19}$$

$$\hat{a}\,|\Psi^0_{\uparrow\downarrow,N}\rangle = \sqrt{N}\,|\Psi_{\uparrow\downarrow,N-1}\rangle\ , \qquad \hat{a}^\dagger\,|\Psi^0_{\uparrow\downarrow,N}\rangle = \sqrt{N+1}\,|\Psi_{\uparrow\downarrow,N+1}\rangle\ . \tag{A20}$$

After calculating the eigenvalues for the Hamiltonian in Eq. (A17), we obtain closed form analytic expressions with energy dispersion

$$\varepsilon_{\{N_0\uparrow,N_0\downarrow,N_0+1\uparrow,N_0+1\downarrow\}}(k,\,\Delta) = \left(N_0+\frac{1}{2}\right)\hbar\omega_0+\mathcal{D}k^2 \pm \sqrt{\mathbb{C}_1(k,\,\Delta)\pm\sqrt{\mathbb{C}_2(k,\,\Delta)}}\ , \tag{A21}$$

$$\mathbb{C}_1(k,\,\Delta) = (\hbar\omega_0/2)^2+\zeta\nu\mathcal{A}\mathcal{D}k^2+\left[\zeta^2\mathcal{D}^2+\mathcal{A}^2(1+5/2\nu^2)\right]k^2\ , \tag{A22}$$

$$\begin{aligned}\mathbb{C}_2(k,\,\Delta) = {}& \zeta^2\mathcal{A}^2\mathcal{D}^2k^4(1+\nu^2)+4\nu(\zeta\nu\mathcal{D}+\mathcal{A})\mathcal{A}^3k^4 \\ & -3\nu(2\zeta\mathcal{D}+\nu\mathcal{A})\mathcal{A}\hbar\omega_0\Delta k^2+4\hbar^2\omega_0^2(\Delta^2+\mathcal{A}^2k^2)\ .\end{aligned} \tag{A23}$$

Taking the limits $\zeta\mathcal{D} \to 0$ and $\nu k \to 0$, we are left with two uncoupled energy subbands

$$\varepsilon_{\{N_0\uparrow,N_0\downarrow\}}(k,\,\Delta) = N_0\,\hbar\omega_0+\mathcal{D}k^2 \pm \sqrt{\Delta^2+\mathcal{A}^2k^2}\ , \tag{A24}$$

$$\varepsilon_{\{N_0+1\uparrow,N_0+1\downarrow\}}(k,\,\Delta) = (N_0+1)\,\hbar\omega_0+\mathcal{D}k^2 \pm \sqrt{\Delta^2+\mathcal{A}^2k^2}\ . \tag{A25}$$

Therefore, we conclude that the effect of electron-photon interaction is quite similar to graphene as far as one photon number N_0 is concerned. The main difference being that the energy gap in the 3DTI is of order $\mathcal{O}(\zeta^2)$, which may be neglected for low intensity light. Consequently, the energy dispersion relation becomes

$$\varepsilon_\beta(k,\,\Delta_0) = N_0\,\hbar\omega_0+\mathcal{D}k^2+\beta\sqrt{\left[\Delta_0+\mathcal{O}(\zeta^2)\right]^2+(\mathcal{A}k)^2}\ , \tag{A26}$$

where $\beta = \pm 1$ and Δ_0 is the photon-induced energy gap as in graphene.

Appendix B: Dressed 3DTI Electron surface states

It follows from Appendix A that the effect due to $\sim \hat{\mathbf{A}}^2$-terms would play a the role only if two optical modes are considered. This effect is of order $\mathcal{O}(\zeta^2)$ and may be neglected in our calculations. When the surface of a 3DTI is irradiated with circularly polarized light, the light will penetrate into the sample and decay exponentially away from the surface, similar to the wave function for a surface electronic state. Therefore, by including this decay effect, the vector potential in Eq. (A2) is generalized as

$$\hat{\mathbf{A}} = \mathcal{F}_0\left(\mathbf{e}_+\hat{a}+\mathbf{e}_-\hat{a}^\dagger\right)\,\mathrm{e}^{-\xi z}\ , \tag{B1}$$

where $1/\xi$ is the decay length. By including the z dependence, the Hamiltonian of the electron system is found to be

$$\hat{\mathcal{H}}_{3D}(\mathbf{k}_\perp,\,z) = \hat{\mathcal{H}}^{(1)}_{3D}(z)+\hat{\mathcal{H}}^{(2)}_{3D}(\mathbf{k}_\perp)\ , \tag{B2}$$

where

$$\hat{\mathcal{H}}^{(1)}_{3D}(z) = \left(\mathcal{C} - \mathcal{D}_z\partial_z^2\right) \overleftrightarrow{\mathbb{I}}_{[4]} + \begin{pmatrix} (\mathcal{M} + \mathcal{B}_z\partial_z^2)\overleftrightarrow{\sigma}_3 - i\mathcal{A}_z\partial_z \overleftrightarrow{\sigma}_1 & 0 \\ 0 & (\mathcal{M} + \mathcal{B}_z\partial_z^2)\overleftrightarrow{\sigma}_3 + i\mathcal{A}_z\partial_z \overleftrightarrow{\sigma}_1 \end{pmatrix} , \tag{B3}$$

$$\hat{\mathcal{H}}^{(2)}_{3D}(\mathbf{k}_\perp) = -\mathcal{D}_\perp k^2 \overleftrightarrow{\mathbb{I}}_{[4]} - \mathcal{B}_\perp k^2 \overleftrightarrow{\sigma}_3 \otimes \overleftrightarrow{\mathbb{I}}_{[2]} + \begin{pmatrix} 0 & \mathcal{A}_\perp k_- \overleftrightarrow{\sigma}_1 \\ \mathcal{A}_\perp k_+ \overleftrightarrow{\sigma}_1 & 0 \end{pmatrix} . \tag{B4}$$

Here, $\mathbf{k}_\perp = (k_x,\, k_y)$, $\mathcal{C}$, $\mathcal{M}$, $\mathcal{A}_z$, $\mathcal{B}_z$, $\mathcal{D}_z$ are parameters in the Kane $\mathbf{k}\cdot\mathbf{p}$ model for bulk states, and $\mathcal{A}_\perp$, $\mathcal{B}_\perp$, $\mathcal{D}_\perp$ are parameters for surface states. We note that the parameter $\mathcal{C}$ may be eliminated by simply shifting the band edges. Since the electron-photon interaction occurs in the region close to the surface, we only need to consider $\hat{\mathcal{H}}^{(2)}_{3D}(\mathbf{k}_\perp)$ in Eq. (B2), which contains the coupling with the incident circularly polarized light.

When $\mathbf{k} = \{\mathbf{k}_\perp,\, k_z\} = 0$, the Hamiltonian in Eq. (B4) plus the single-photon energy as well as the light-electron coupling together give

$$\hat{\mathcal{H}}_{\mathbf{k}=0} = \hbar\omega_0\, \hat{a}^\dagger\hat{a} + 2\zeta\mathcal{A}_\perp \begin{pmatrix} 0 & \begin{smallmatrix} 0 & \hat{a} \\ \hat{a} & 0 \end{smallmatrix} \\ \begin{smallmatrix} 0 & \hat{a}^\dagger \\ \hat{a}^\dagger & 0 \end{smallmatrix} & 0 \end{pmatrix} . \tag{B5}$$

By introducing a small dimensionless parameter $\alpha' = 2\zeta\mathcal{A}_\perp/\mathcal{M} \ll 1$, and the two matrices

$$\overleftrightarrow{\Gamma}_+ = \overleftrightarrow{\sigma}_+ \otimes \overleftrightarrow{\sigma}_1 = \begin{pmatrix} 0 & \begin{smallmatrix} 0 & 1 \\ 1 & 0 \end{smallmatrix} \\ \begin{smallmatrix} 0 & 0 \\ 0 & 0 \end{smallmatrix} & 0 \end{pmatrix} , \qquad \hat{\Gamma}_- = \overleftrightarrow{\sigma}_- \otimes \overleftrightarrow{\sigma}_1 = \begin{pmatrix} 0 & \begin{smallmatrix} 0 & 0 \\ 0 & 0 \end{smallmatrix} \\ \begin{smallmatrix} 0 & 1 \\ 1 & 0 \end{smallmatrix} & 0 \end{pmatrix} , \tag{B6}$$

the Hamiltonian in Eq. (B5) may be rewritten compactly as

$$\hat{\mathcal{H}}_{\mathbf{k}=0} = \hbar\omega_0\, \hat{a}^\dagger\hat{a} + \alpha'(\overleftrightarrow{\Gamma}_-\hat{a}^\dagger + \overleftrightarrow{\Gamma}_+\hat{a}) . \tag{B7}$$

In analogy with Eq. (A9), we construct a basis set containing four states, i.e., $|++\rangle = |1,0,0,0\rangle$, $|+-\rangle = |0,1,0,0\rangle$, $|-+\rangle = |0,0,1,0\rangle$, $|--\rangle = |0,0,0,1\rangle$. For this basis set, it is a simple matter to show the following properties

$$\begin{gathered} \hat{a}^\dagger\,|N,\pm\pm\rangle = \sqrt{N+1}\,|N+1,\pm\pm\rangle, \\ \hat{a}\,|N,\pm\pm\rangle = \sqrt{N}\,|N-1,\pm\pm\rangle, \\ \overleftrightarrow{\Gamma}_+\,|N,+\pm\rangle = 0 , \qquad \overleftrightarrow{\Gamma}_+|N,+\pm\rangle = 0 , \\ \overleftrightarrow{\Gamma}_+\,|N,-\pm\rangle = |N,+\mp\rangle , \qquad \overleftrightarrow{\Gamma}_-|N,+\mp\rangle = |N,-\pm\rangle . \end{gathered} \tag{B8}$$

We may also expand the dressed electronic states at $\mathbf{k} = 0$ over this basis set leading to

$$\begin{aligned} |\Psi^0_{++,N}\rangle &= \mu_{N,+}|++,N\rangle + \nu_{N,+}|+-,N\rangle + \nu_{N+1,-}|-+,N+1\rangle + \nu_{N+1,-}|--,N+1\rangle , \\ |\Psi^0_{+-,N}\rangle &= \nu_{N,+}|++,N\rangle + \mu_{N,+}|+-,N\rangle + \nu_{N+1,-}|-+,N+1\rangle + \nu_{N+1,-}|--,N+1\rangle , \\ |\Psi^0_{-+,N}\rangle &= \nu_{N,+}|++,N\rangle + \nu_{N,+}|+-,N\rangle + \mu_{N+1,-}|-+,N+1\rangle + \nu_{N+1,-}|--,N+1\rangle , \\ |\Psi^0_{--,N}\rangle &= \nu_{N,+}|++,N\rangle + \nu_{N,+}|+-,N\rangle + \nu_{N+1,-}|-+,N+1\rangle + \mu_{N+1,-}|--,N+1\rangle . \end{aligned}$$

For $N \gg 1$ and $\alpha' \ll 1$, calculation shows that

$$\mu_{N,+} \simeq \mu_{N,-} \simeq \mu_{N+1,+} \simeq \mu_{N+1,-} \simeq 1 - \left(\frac{\alpha'}{2}\right)^2 , \tag{B9}$$

$$\nu_N \simeq \nu_{N,-} \simeq \nu_{N+1.+} \simeq \nu_{N+1,-} \simeq \frac{\alpha'}{2} . \tag{B10}$$

Introducing the pair of operators

$$\overleftrightarrow{\Gamma}_{12} = \begin{pmatrix} 0 & 1 & 0 \\ 0 & 0 & \\ 0 & & 0 \end{pmatrix} , \qquad \overleftrightarrow{\Gamma}_{34} = \begin{pmatrix} 0 & & 0 \\ & 0 & 1 \\ 0 & 0 & \end{pmatrix} , \tag{B11}$$

we obtain

$$\overleftrightarrow{\Gamma}_{12} \left| N, +- \right\rangle = \left| N, ++ \right\rangle , \qquad \overleftrightarrow{\Gamma}_{34} \left| N, ++ \right\rangle = \left| N, +- \right\rangle , \tag{B12}$$

$$\overleftrightarrow{\Gamma}_{34} \left| N, -+ \right\rangle = \left| N, -- \right\rangle , \qquad \overleftrightarrow{\Gamma}_{12} \left| N, -- \right\rangle = \left| N, -+ \right\rangle . \tag{B13}$$

For the Hamiltonian in Eq. (A7) within the 2×2 subspace, as a special case, we introduce

$$\overleftrightarrow{\sigma}_{+} = \overleftrightarrow{\Gamma}_{12} , \qquad \overleftrightarrow{\sigma}_{-} = \overleftrightarrow{\Gamma}_{34} . \tag{B14}$$

Finally, we can rewrite the full Hamiltonian in Eq. (B2) for $\mathbf{k} \neq 0$, using the basis set $|N_0, \pm\pm\rangle$, as

$$\hat{\mathcal{H}}_{3D}(\mathbf{k}_{\perp}, z) = N_0 \, \hbar\omega_0 + \left(\begin{array}{cc|cc} \mathcal{C}_+ - \mathcal{D}_{z,-}\partial_z^2 - \mathcal{D}_{\perp,-}k^2 - \Delta & -i\mathcal{A}_z\partial_z & 0 & \mathcal{A}_\perp k_- \\ -i\mathcal{A}_z\partial_z & \mathcal{C}_- - \mathcal{D}_{z,+}\partial_z^2 - \mathcal{D}_{\perp,+}k^2 - \Delta & \mathcal{A}_\perp k_- & 0 \\ \hline \mathcal{A}_\perp k_+ & \mathcal{C}_+ - \mathcal{D}_{z,-}\partial_z^2 - \mathcal{D}_{\perp,-}k^2 + \Delta & i\mathcal{A}_z\partial_z & \\ \mathcal{A}_\perp k_+ & 0 & i\mathcal{A}_z\partial_z & \mathcal{C}_- - \mathcal{D}_{z,+}\partial_z^2 + \mathcal{D}_{\perp,+}k^2 + \Delta \end{array} \right) , \tag{B15}$$

where the $\pm$ signs correspond to opposite pseudo-spins in the basis set. Making use of Eq. (B15), we obtain the secular equation for the energy dispersion relations when $\Delta = 0$, that is,

$$\varepsilon^2 - \mathcal{A}_\perp^2 k^2 + \mathbb{N}_1\mathbb{N}_1 + \mathcal{A}_z^2\xi^2 + \mathcal{D}_-\mathbb{N}_1\xi^2 + \mathcal{D}_+\mathbb{N}_2\xi^2 + \mathcal{D}_- + \mathcal{D}_+\mathbb{N}_2\xi^2 + \mathcal{D}_+\mathcal{D}_-\xi^4 - (\mathbb{N}_1 + \mathbb{N}_2 + 2\mathcal{D}\xi^2)\,\varepsilon = 0 , \tag{B16}$$

where we have introduced the notations

$$\mathbb{N}_{1,2}(k) = \mathcal{C} \pm \mathcal{M} + (\mathcal{D}_\perp \mp \mathcal{B}_\perp)\, k^2 , \tag{B17}$$

$$\mathcal{D}_\pm = \mathcal{D}_z \pm \mathcal{B}_z . \tag{B18}$$

[1] M. Z. Hasan and C. L. Kane. *Colloquium* : Topological insulators. *Rev. Mod. Phys.*, 82:3045–3067, Nov 2010.

[2] X.-L. Qi and S.-C. Zhang. Topological insulators and superconductors. *Rev. Mod. Phys.*, 83:1057–1110, Oct 2011.

[3] B.A. Bernevig, T. A. Hughes, and S.-C. Zhang. Quantum spin hall effect and topological phase transition in hgte quantum wells. *Science*, 314:1751–1761, Dec. 2006.

[4] Geim A. K. Morozov S. V. Jiang D. Katsnelson M. I. Grigorieva I. V. Dubonos S. V. Firsov A. A. Novoselov, K. S. Two-dimensional gas of massless dirac fermions in graphene. *Nature*, 438(197), 2005.

[5] A. K. Geim. Graphene: Status and prospects. *Science*, 324(5934), 2009.

[6] W.-Y. Shan, H.-Z Lu, and S.-Q. Shen. Effective continuous model for surface states and thin films of three-dimensional topological insulators. *New Journal of Physics*, 12(4):043048, 2010.

[7] B. Zhou, H.-Z. Lu, R.-L. Chu, S.-Q. Shen, and Q. Niu. Finite size effects on helical edge states in a quantum spin-hall system. *Phys. Rev. Lett.*, 101:246807, Dec 2008.

[8] T. Oka and H. Aoki. Photovoltaic hall effect in graphene. *Phys. Rev. B*, 79(8):081406, 2009.

[9] O. V. Kibis. Metal-insulator transition in graphene induced by circularly polarized photons. *Phys. Rev. B*, 81(16):165433, 2010.

[10] O. V. Kibis, O. Kyriienko, and I. A. Shelykh. Band gap in graphene induced by vacuum fluctuations. *Phys. Rev. B*, 84:195413, Nov 2011.

[11] O. V. Kibis. Dissipationless electron transport in photon-dressed nanostructures. *Phys. Rev. Lett.*, 107:106802, Aug 2011.

[12] M. I. Katsnelson, K. S. Novoselov, and A. K. Geim. Chiral tunnelling and the klein paradox in graphene. *Nat Phys*, 2:620–625, 2006.

[13] Iurov A, G. Gumbs, O. Roslyak, and D. H. Huang. Anomalous photon-assisted tunneling in graphene. *Journal of Physics: Condensed Matter*, 24(1):015303, 2012.
[14] S. Mondal, D. Sen, K. Sengupta, and R. Shankar. Magnetotransport of dirac fermions on the surface of a topological insulator. *Phys. Rev. B*, 82:045120, Jul 2010.
[15] D. Culcer, E. H. Hwang, T. D. Stanescu, and S. Das Sarma. Two-dimensional surface charge transport in topological insulators. *Phys. Rev. B*, 82:155457, Oct 2010.
[16] A. H. Castro Neto, F. Guinea, N. M. R. Peres, K. S. Novoselov, and A. K. Geim. The electronic properties of graphene. *Rev. Mod. Phys.*, 81(1):109–162, 2009.
[17] Y. Tanaka, T. Yokoyama, and N. Nagaosa. Manipulation of the majorana fermion, andreev reflection, and josephson current on topological insulators. *Phys. Rev. Lett.*, 103:107002, Sep 2009.
[18] M. Barbier, P. , Vasilopoulos, and F. M. Peeters. Single-layer and bilayer graphene superlattices: collimation, addition dirac points and dirac lines. *Philosophical Transactions of Royal Society A*, 386:5499–5524, 2010.
[19] J. Tworzydło, B. Trauzettel, M. Titov, A. Rycerz, and C. W. J. Beenakker. Sub-poissonian shot noise in graphene. *Phys. Rev. Lett.*, 96:246802, Jun 2006.
[20] Siegfried Flügge. Practical quantum mechanics. *Springer Study Edition.*, 2009.
[21] M. König, H. Buhmann, L. W. Molenkamp, T. Hughes, C.-X. Liu, X.-L. Qi, and S.-C. Zhang. The quantum spin hall effect: Theory and experiment. *Journal of the Physical Society of Japan*, 77(3):031007, 2008.
[22] L. Brey and H. A. Fertig. Electronic states of graphene nanoribbons studied with the dirac equation. *Phys. Rev. B*, 73:235411, Jun 2006.
[23] O Roslyak, A Iurov, Godfrey Gumbs, and Danhong Huang. Unimpeded tunneling in graphene nanoribbons. *Journal of Physics: Condensed Matter*, 22(16):165301, 2010.
[24] Christopher Gerry and Peter Knight. Introductory quantum optics. *Cambridge University Press*, 2005.